



X-ray polarization observations of IC 4329A with IXPE: Constraining the geometry of X-ray corona

INDRANI PAL^{1,*}, C. S. STALIN¹, RWITIKA CHATTERJEE² and VIVEK K. AGRAWAL²

¹Indian Institute of Astrophysics, Block II, Koramangala, Bangalore 560034, India.

²Space Astronomy Group, ISITE Campus, U. R. Rao Satellite Centre, Bangalore 560037, India.

*Corresponding author. E-mail: indrani.pal@iiap.res.in

MS received 17 May 2023; accepted 14 August 2023

Abstract. X-ray polarimetry is a powerful tool to probe the geometry of the hot X-ray corona in active galactic nuclei (AGN). Here, we present our results on the characterization of the X-ray polarization of the radio-quiet Seyfert-type AGN IC 4329A at a redshift of $z = 0.016$. This is based on observations carried out by the Imaging X-ray Polarimeter (IXPE). IXPE observed IC 4329A during 5–15 January 2023, for a total observing time of 458 ks. From the model-independent analysis, we found a polarization degree (Π_X) of $3.7 \pm 1.5\%$ and a polarization position angle (Ψ_X) of $61^\circ \pm 12^\circ$ in the 2–8 keV energy range (at 68% confidence). This is also in agreement with the values of Π_X and Ψ_X of $4.7 \pm 2.2\%$ and $71^\circ \pm 14^\circ$, respectively, obtained from spectro-polarimetric analysis of the I, Q and U Stokes spectra in the 2–8 keV energy band (at 90% confidence). The value of Π_X in the 2–8 keV band obtained from the model-independent analysis is lower than the minimum detectable polarization (MDP) value of 4.5%. However, Π_X obtained from spectro-polarimetric analysis in the 2–8 keV band is larger than the MDP value. In the 3–5 keV band, we found Π_X of 6.5 ± 1.8 , which is larger than the MDP value of 5.5%. The observed moderate value of Π_X obtained from the analysis of the IXPE data in the 3–5 keV band argues against a spherical lamp-post geometry for the X-ray corona in IC 4329A; however, considering simulations, the observed polarization measurements tend to favor a conical shape geometry for the corona. This is the first time measurement of X-ray polarization in IC 4329A. Measurements of the X-ray polarization in many such radio-quiet AGN will help in constraining the geometry of the X-ray corona in AGN.

Keywords. Galaxies: active—galaxies: seyfert—individual: IC 4329A.

1. Introduction

Active galactic nuclei (AGN), one among the luminous objects in the Universe, are believed to be powered by the accretion of matter onto super-massive black holes (SMBHs; $\sim 10^6$ – $10^{10} M_\odot$) situated at the centers of galaxies (Lynden-Bell 1969; Shakura & Sunyaev 1973; Rees 1984; Antonucci 1993; Urry & Padovani 1995). They emit over the entire accessible electromagnetic spectrum, such as the high energy γ -rays (Hartman *et al.* 1999), X-rays (Fabian 2012), ultra-violet (UV) (Murray *et al.* 1995), optical (Boroson & Green 1992), infrared (Sanders & Mirabel 1996) and radio (Condon *et al.* 1991). The AGN come under two broad categories, a majority of them emit less or no radio emission and are called radio-quiet AGN, while a minority of about 10% emit copiously in the radio band and are called

radio-loud AGN (Kellermann *et al.* 1989). Though X-rays are emitted by the different classes of AGN, the detailed physics of the cause of X-ray emission needs to be more understood and is highly debated. Also, the relative contribution of the physical processes to the X-ray emission may differ between the different AGN classes (Padovani 2017).

In the radio-quiet category of AGN, the observed X-ray emission is believed to be due to inverse Compton scattering of optical-UV radiation from the accretion disk by hot electrons ($\sim 10^{8-9}$ K) in the corona, a constituent of AGN (Haardt & Maraschi 1991, 1993; Haardt *et al.* 1994). The X-ray corona is believed to be located close to the accretion disk, with microlensing studies pointing it to be compact with the size of a few gravitational radii ($r_g = GM/c^2$; Chartas *et al.* 2016). X-ray reverberation mapping studies also indicate the

corona to be compact and of the order of 3–10 r_g in radius (Fabian *et al.* 2009). In the case of radio-loud category of AGN with relativistic jets, the X-ray from the jets will have a major contribution to the observed X-rays (Padovani 2017), with an insignificant contribution from the corona (Fedorova *et al.* 2022).

Recent studies, most notably using observations from the Nuclear Spectroscopic Telescope Array (NuSTAR, Harrison *et al.* 2013) were able to characterize the nature of the corona in AGN, such as its temperature (kT_e) and variation in its temperature (Ursini *et al.* 2015, 2016; Keek & Ballantyne 2016; Zoghbi *et al.* 2017; Kang *et al.* 2021; Pal *et al.* 2022a,b; Pal & Stalin 2023). This is achieved via modeling of their broadband X-ray spectra, as the shape of the primary X-ray continuum in AGN is sensitive to the temperature of the coronal plasma, its optical depth, geometry of the corona and nature of the seed photons (Haardt & Maraschi 1993; Haardt *et al.* 1994).

The corona could be either a spherical structure above the black hole (spherical lamp-post; Fabian *et al.* 2017) or a slab-like structure sandwiching the accretion disk (Haardt & Maraschi 1993) or a conical structure (Ursini *et al.* 2021). From the physical model fits to the observed high energy spectra of AGN, the kT_e reported in the literature assumes the corona to have either a spherical or a slab geometry (Rani & Stalin 2018). Also, from the multi-epoch spectral analysis available in the literature, several models of the corona, including changes in the structure of the corona, are proposed to explain the observed changes in kT_e (Pal *et al.* 2022a; Pal & Stalin 2023). However, from spectral analysis of AGN, it is not easy to distinguish between different coronal geometries (Tortosa *et al.* 2018; Middei *et al.* 2019). Irrespective of several studies in the literature attempting to characterize the corona in AGN, we still need to gain knowledge on (i) origin of the corona, (ii) cause of its high temperature and (iii) its geometry.

X-ray polarimetric observations can yield the needed measurement to constrain the geometry of the X-ray-emitting corona in AGN (Matt *et al.* 1989, 1993). This is because polarization depends on geometry of the emitting region and the external photon field (Tamborra *et al.* 2018; Zhang *et al.* 2019). The launch of the Imaging X-ray Polarimetry Explorer (IXPE; Weiskopf *et al.* 2022) on 9 December 2021, sensitive in 2–8 keV band has enabled the studies of X-ray polarization from AGN. As of now, IXPE has observed four radio-quiet AGN, namely MCG-05-23-16, the Circinus galaxy, NGC 4151 and IC 4329A. Of these, for MCG-05-23-16, Marinucci *et al.* (2022), reported a polarization degree $\Pi_X < 4.7\%$. In the case of the

Circinus Galaxy, Ursini *et al.* (2023), reported a high value of $\Pi_X = 28\%$, which is thought to be due to reflection from the torus. For NGC 4151, Gianolli *et al.* (2023), found values of Π_X and Ψ_X of $4.9 \pm 1.1\%$ and $86^\circ \pm 7^\circ$, respectively, arguing for a slab geometry of the corona. Here, we reported the results of polarization on the fourth radio-quiet AGN, IC 4329A.

IC 4329A with a black hole mass of $6.8_{-1.1}^{+1.2} \times 10^7 M_\odot$ (Bentz *et al.* 2023) is one of the brightest Seyfert 1.2 galaxies (Véron-Cetty & Véron 2010) in X-rays at a redshift $z = 0.016$ (Willmer *et al.* 1991) with an X-ray spectrum having many absorbing systems (Steenbrugge *et al.* 2005). It is an ideal object to study the intrinsic continuum and reflection from any material surrounding the source. It has been studied extensively for its X-ray spectral and timing properties (Dewangan *et al.* 2021). Observations of IC 4329A in millimeter were explained as due to synchrotron emission in the hot corona (Inoue & Doi 2018). From Comptonization model fits to the NuSTAR observations on IC 4329A, Lubiński *et al.* (2016), reported a kT_e of 40_{-5}^{+7} keV using the COMPPOS model, assuming a spherical geometry of the corona. Alternatively, Petrucci *et al.* (2001), using the Comptonization model and a slab geometry of the corona, found a value of $kT_e = 170_{-5}^{+10}$ keV from the analysis of the BeppoSAX data. Tortosa *et al.* (2018) reported $kT_e = 37 \pm 7$ keV from fitting compTT to the source spectrum for slab geometry. Kang & Wang (2022) estimated $kT_e = 71_{-15}^{+37}$ keV using relxillCP model. Kamraj *et al.* (2022) also found $kT_e = 82_{-7}^{+16}$ keV from xillverCP fit to the source spectrum. We analysed the NuSTAR spectrum taken in 2012. Fitting the spectrum using xillverCP, we obtained best-fit values of Γ and kT_e of $1.83_{-0.003}^{+0.003}$ and 64_{-12}^{+15} keV, respectively (Pal *et al.* 2023, under preparation). From a joint fit of XMM-Newton EPIC PN and NuSTAR spectra observed simultaneously on 12 August 2021, we found $\Gamma = 1.88_{-0.01}^{+0.01}$ and $kT_e > 135$ keV. The best-fit model with data and the residues are given in Figure 1. All the spectral fits produced good fit statistics with $\chi^2/dof \sim 1.0$, irrespective of the coronal geometry assumed in the used models. Thus, from the analysis of AGN X-ray continuum, it is not possible to constrain the geometry of the corona, while X-ray polarimetric observations could provide the needed constraint on the coronal geometry. Here, we presented our results on the analysis of the first X-ray polarimetric observations carried out on this source by IXPE. The observations and data reduction are described in Section 2, the analysis is described in Section 3, and the results are discussed in Section 4, followed by the summary in Section 5.

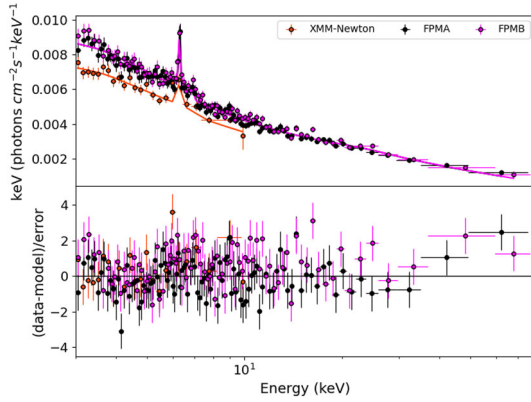


Figure 1. XMM-Newton EPIC PN, NuSTAR FPMA and FPMB spectra fitted jointly in 3–78 keV energy band using the model $\text{const} \times \text{TBabs} \times \text{zTBabs} \times (\text{xillverCP})$. The observations were taken simultaneously on 12 August 2021.

Table 1. Log of IXPE observation.

OBSID	Date	Exposure time (s)
01003601	2023-01-05	457715

2. Observations and data reduction

IXPE (Weisskopf *et al.* 2022) observed IC 4329A during 5–15 January 2023, with its three detector units (DUs) for a net exposure of about 458 ks. The IXPE observation log is given in Table 1. The calibrated data were produced by the standard IXPE pipeline provided by the Science Operation Center (SOC).¹ We used the cleaned and calibrated level 2 data for the scientific analysis.

The publicly available level 2 data were analysed using IXPEOBSSIM software v30.0.0 (Baldini *et al.* 2022). A count map in sky coordinates was generated using the CMAP algorithm within the `xpbin` task. We adopted a circular region with a radius of 70'' for the source extraction from the three DUs, and a source-free region with a radius of 100'' was chosen for the background extraction for each DU. We then used the `xpselect` task to generate the filtered source and background regions. For the spectro-polarimetric analysis, the I, Q and U source and background spectra were generated using the PHA1, PHA1Q and PHA1U algorithm using `xpbin` task within IXPEOBSSIM for the three DUs. We used a minimum of 30 counts per bin

¹<https://heasarc.gsfc.nasa.gov/docs/ixpe/analysis/IXPE-SOC-DOC-009-UserGuide-Software.pdf>.

Table 2. Polarization parameters in different energy bands. The errors are quoted at 68% confidence

Energy band (keV)	$\Pi_X \pm \delta\Pi_X$ (%)	MDP (%)	$\Psi_X \pm \delta\Psi_X$ (°)
2–8	3.7 ± 1.5	4.5	61 ± 12
2–3	3.6 ± 1.8	5.5	66 ± 14
3–5	6.5 ± 1.8	5.5	74 ± 8
5–8	5.4 ± 3.5	10.73	21 ± 19

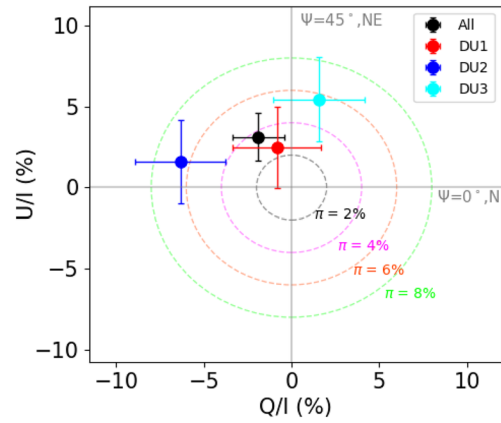


Figure 2. Normalized U/I and Q/I Stokes parameters in the total 2–8 keV band of IXPE. The plotted errors are the 68% uncertainties, and the concentric circles correspond to different values of polarization degree.

to bin the I spectra, where a constant energy binning of 0.2 keV was used for Q and U spectra.

3. Analysis

3.1 Polarimetry

The polarimetric signal from IC 4329A was analysed using the PCUBE algorithm in the `xpbin` task. The three polarization cubes for the three DUs were generated to extract information like the Stokes parameters (I, Q, U); the minimum detectable polarization (MDP); polarization degree (Π_X); polarization angle (Ψ_X) and their associated errors. We first generated the three polarization cubes corresponding to three DUs in the entire 2–8 keV energy band. The combined polarization parameters from the three DUs in the 2–8 keV band are given in Table 2. We found $\Pi_X = 3.7 \pm 1.5\%$, $\text{MDP} = 4.5\%$ and $\Psi_X = 61^\circ \pm 12^\circ$. The normalized U/I and Q/I Stokes parameters obtained from the three polarization cubes corresponding to the three DUs and the combined cube are shown in Figure 2.

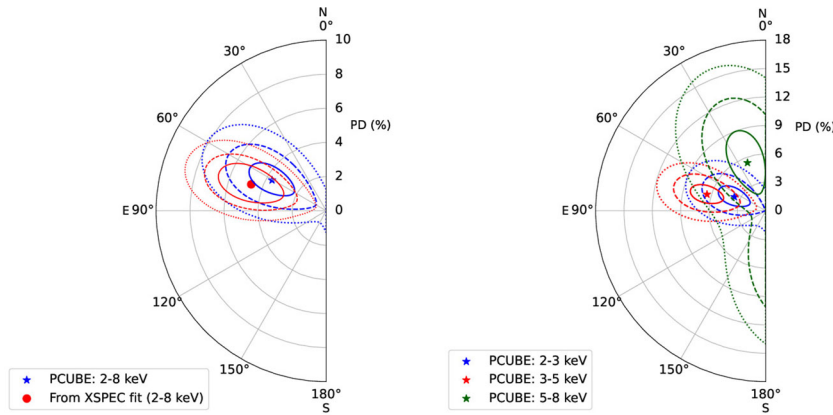


Figure 3. The 68%, 90% and 99% confidence contours between Π_X and Ψ_X in the 2–8 keV (left panel) band and in three different energy bands (right panel).

To check for the energy dependence of the polarization parameters, we also derived the polarization parameters in three energy bins of 2–3, 3–5 and 5–8 keV using the PCUBE algorithm. The derived parameters are given in Table 2. The polarization contours for the total energy range of 2–8 keV and for the different energy ranges are given in Figure 3. From Table 2 and Figure 3, it is evident that Π_X and Ψ_X are consistent within errors in the energy range of 2–3, 3–5 and 2–8 keV, while there is a tendency for a decrease in Ψ_X in the 5–8 keV band. However, the error is so large to arrive at any firm conclusion on the Ψ_X change at the higher energy band.

Though the values of Π_X in the 2–3, 5–8 and 2–8 keV bands are close to or lower than the MDP values, at 3–5 keV, we found a Π_X of $6.5 \pm 1.8\%$, which is larger than the MDP value of 5.5%. We thus conclude to have detected significant X-ray polarization in IC 4329A, and this is the first report of the detection of the X-ray polarization signal in IC 4329A.

3.2 Spectro-polarimetry

We carried out the spectro-polarimetric analysis of the IXPE I, Q, U spectra in the 2–8 keV energy band. For the spectral fitting, we used an absorbed powerlaw, modified by a multiplicative constant polarization model polconstant in XSPEC V12.13.0c (Arnaud 1996). This model assumes a constant polarization degree and angle over the specific energy band. In XPSEC, the model takes the following form:

$$\text{constant} \times \text{TBabs} \times \text{zTBabs} \times (\text{polconst} \times \text{po}). \quad (1)$$

Here, the ‘const’ represents the inter-calibration constant for each detector, which varies between 0.95 and

1.00. TBabs was used to model the Milky Way Galactic hydrogen column density, which was taken from Willingale *et al.* (2013). To model the host galaxy column density, we used zTBabs and let the column density (N_H) vary during the fit. This model fits the I, Q and U spectra (from the three detectors) well with a reduced chi-square ($\Delta\chi^2 = 1083/1064$). The best fit I, Q and U spectra with the residues are given in Figure 4. The spectro-polarimetric fit produced a Π_X of $4.7 \pm 2.2\%$ (larger than the MDP value of 4.5%) and Ψ_X of $71^\circ \pm 14^\circ$ associated with the primary emission when modeled with a power law of photon index (Γ) of 1.95 ± 0.05 . In Figure 3, the contours between Π_X and Ψ_X in 68%, 90% and 99%, are plotted along with the contours obtained from the polarimetric analysis. All the model parameters for each of the detectors were tied during the fit. The errors were calculated at the 90% confidence ($\chi^2 = 2.71$ criterion). The best-fit parameters are given in Table 3.

We also analysed Markov Chain Monte Carlo (MCMC) using the XSPEC EMCEE code.² We used the Goodman–Weare algorithm by specifying 20 walkers with 1,00,000 iterations and an initial chain burn of 8000 to calculate the probability distribution function of the model parameters and their associated uncertainties. The mean of the Probability distributions of the model parameters with the associated errors from the MCMC analysis are also reported in Table 3.

4. Discussion

The measured polarized X-ray emission in the radio-quiet category of AGN is believed to be due to the

²<https://github.com/jeremysanders/xspecemcee>.

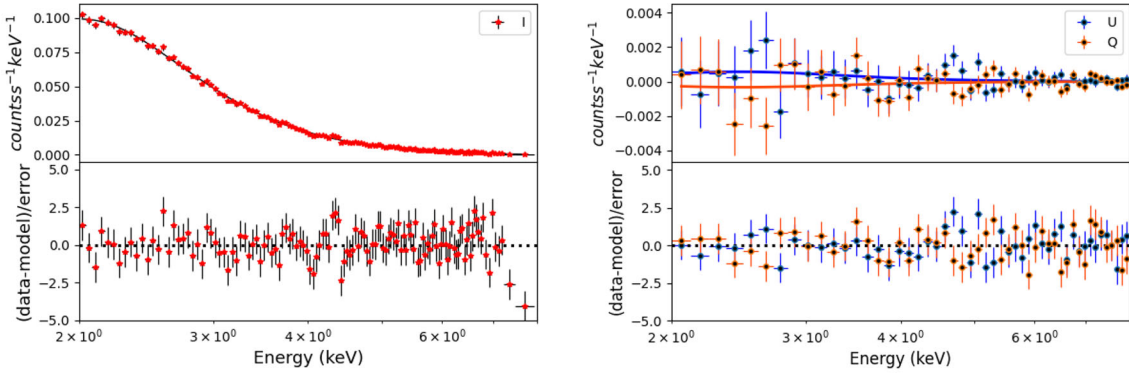


Figure 4. Left panel: IXPE I Stokes best-fit spectra with residuals. Right panel: Q and U Stokes best-fit spectra with residuals.

Table 3. Results of spectro-polarimetric analysis.

Parameters	XSPEC analysis	MCMC analysis
N_H ($\times 10^{22}$ cm $^{-2}$)	$0.70^{+0.12}_{-0.12}$	$0.70^{+0.12}_{-0.11}$
Π_X (%)	$4.7^{+2.2}_{-2.2}$	$4.6^{+2.0}_{-2.4}$
Ψ_X ($^\circ$)	71^{+14}_{-14}	70^{+14}_{-15}
Γ	$1.95^{+0.05}_{-0.05}$	$1.95^{+0.05}_{-0.05}$
N	$0.023^{+0.002}_{-0.002}$	$0.023^{+0.002}_{-0.002}$

inverse Compton scattering of UV/optical accretion disk photons by hot electrons in the corona. Therefore, the measured degree of X-ray polarization depends on the geometry of the corona. We examined the polarimetric properties of the Seyfert 1 galaxy IC 4329A using the IXPE data through a model-independent and spectro-polarimetric analysis. Using the model-independent approach in the 2–8 keV, we found a polarization angle of $61^\circ \pm 12^\circ$ and a polarization degree of $3.7 \pm 1.5\%$, which are slightly lower than the MDP value of 4.5% (at 68% confidence level). From spectro-polarimetric analysis, we found values of Π_X and Ψ_X of $4.7 \pm 2.2\%$ (larger than the MDP value of 4.5%) and $71^\circ \pm 14^\circ$, respectively. Recently, Ursini et al. (2021) simulated polarization signals expected from AGN corona for three different geometries, namely, slab (inner radius $\sim 10 r_g$), spherical lamp-post (radius $\sim 10 r_g$ and height $\sim 30 r_g$ above the accretion disk) and the truncated cone geometry for an outflowing corona (a failed jet with an outflowing velocity of 0.3 c and initial radius of 20–30 r_g). We claimed that the polarization degree goes up to 12% for a slab coronal geometry. For the symmetrical nature of a spherical lamp-post corona, the polarization signal received from such sources is expected to

be lower than the slab. For such geometries, a very low polarization degree ($\sim 1\text{--}3\%$) is expected (Poutanen & Svensson 1996; Tamborra et al. 2018). For the conical corona, the expected polarization could be between the slab and spherical ones. From their simulation using the MONK (Zhang et al. 2019) code, Ursini et al. (2021) also reported that the polarization angle is close to 180° for slab geometry, while for the spherical and conical geometries, it is scattered around 90° . Our measured value of $\Pi_X = 6.5 \pm 1.8\%$ in the 3–5 keV bands, larger than the MDP value of 5.5%, rules out spherical lamp-post geometry for the corona. However, compared with the simulations of Ursini et al. (2021), our measured values argue for a conical geometry for the corona in IC 4329A. Recently, from simulations, to explain the high Π_X observed in the black hole X-ray binary Cygnus X-1, Poutanen et al. (2023) have shown that a static slab corona can produce Π_X of 4% only at inclinations exceeding 60° . However, an outflowing corona with a high terminal velocity ($\beta_0 > 0.6$) can produce Π_X of around 4% at the line of sight disk inclination $< 30^\circ$. From the spectroscopic analysis of Fe-line in IC 4329A, McKernan & Yaqoob (2004) reported a disk inclination angle of 24^{+9}_{-1} for IC 4329A. Thus, comparing our observed polarization parameters with that expected from simulations (Ursini et al. 2021; Poutanen et al. 2023), we concluded that in IC 4329A, a corona with conical geometry is preferred over a static slab corona. Recently, Ingram et al. (2023) presented the spectro-polarimetric analysis of IC 4329A using observations from XMM-Newton, NuSTAR and IXPE data. The observations from XMM-Newton and NuSTAR were taken during the IXPE observation period. We concluded that though their estimated values of Π_X and Ψ_X tentatively favor an outflowing coronal geometry, however, at the 3σ level, the coronal geometry is unconstrained from our observations.

5. Conclusions

We analysed the first X-ray polarimetric observations of IC 4329A by IXPE. The observation for 458 ks was taken during 5–15 January 2023. The findings of the polarimetric study are as follows:

1. From a model-independent analysis, we found a value of $\Pi_X = 3.7 \pm 1.5\%$ and $\Psi_X = 61^\circ \pm 12^\circ$ in the 2–8 keV band. This value of Π_X is slightly lower than the MDP value of 4.5%.
2. From the spectro-polarimetric analysis of model fits to the spectra, we found values of Π_X and Ψ_X of $4.7 \pm 2.2\%$ and $71^\circ \pm 14^\circ$, respectively, in the 2–8 keV band. Thus, the polarimetric measurements obtained from both model-independent and spectro-polarimetric analyses agree with each other. Also, the value of Π_X obtained from the model fit to the spectrum is larger than the MDP value of 4.5%.
3. We derived the polarization parameters in different energy bands to check for energy-dependent polarization. While Π_X is found to be similar within error bars in all the energy bands, the derived values of Ψ_X are found to agree within errors in the 2–3, 3–5 and 2–8 keV bands. There is a tendency for lower values of Ψ_X in the higher energy range of 5–8 keV. However, the error bar is too large in this energy range. Our observations do not find evidence of changes in polarization between energy bands.
4. In the 3–5 keV band, from model-independent analysis, we found a Π_X of $6.5 \pm 1.8\%$, which is larger than the MDP value of 5.5%. Also, from spectro-polarimetric analysis in the 2–8 keV band, we found a Π_X of $4.7 \pm 2.2\%$, which is larger than the MDP at that energy band. We, therefore, conclude to have detected X-ray polarization in IC 4329A.
5. Our observations, when compared with Monte-Carlo simulations in the literature (Ursini *et al.* 2021), rule out a spherical lamphy-post geometry for the corona in IC 4329A, instead tend to favor a corona with a conical geometry in IC 4329A.

With the results reported in this work, the number of Seyfert type AGN with measured X-ray polarization measurements from IXPE observations have increased to four. X-ray polarimetric observations of more Seyfert-type AGN are needed to put better constraints on the geometry of the X-ray corona in AGN. Also, repeated observations of the same source by IXPE would enable one to constrain for variations in the geometry of the corona, as has been hinted at from spectral modeling of the X-ray spectra of AGN (Keek & Ballantyne 2016; Kang *et al.* 2021; Pal *et al.* 2022a, b).

Acknowledgements

We thank the anonymous referee for her/his valuable comments and suggestions which improved the quality and clarity of the paper. The Imaging X-ray Polarimetry Explorer (IXPE) is a joint US and Italian mission. The US contribution is supported by the National Aeronautics and Space Administration (NASA) and led and managed by its Marshall Space Flight Center (MSFC), with industry partner Ball Aerospace (contract NNM15AA18C). The Italian contribution is supported by the Italian Space Agency (Agenzia Spaziale Italiana, ASI) through contract ASI-OHBI-2017-12-I.0, agreements ASI-INAF-2017-12-H0 and ASI-INFN-2017.13-H0, and its Space Science Data Center (SSDC) with agreements ASI-INAF-2022-14-HH.0 and ASI-INFN 2021-43-HH.0, and by the Istituto Nazionale di Astrofisica (INAF) and the Istituto Nazionale di Fisica Nucleare (INFN) in Italy. This research used data products provided by the IXPE Team (MSFC, SSDC, INAF and INFN). The High-Energy Astrophysics Science Archive Research Center (HEASARC) at NASA Goddard Space Flight Center (GSFC) distributed it with additional software tools. Part of the French contribution is supported by the Scientific Research National Center (CNRS) and the French Space Agency (CNES). We thank the NuSTAR Operations, Software and Calibration teams for the support with the execution and analysis of these observations. This research has used of archival data of XMM-Newton and NuSTAR observatories through the High Energy Astrophysics Science Archive Research Center Online Service, provided by the NASA Goddard Space Flight Center.

References

- Antonucci R. 1993, *Ann. Rev. Astron. Astrophys.*, 31, 473
 Arnaud K. A. 1996, *Astronomical Society of the Pacific Conference Series*, Vol. 101, XSPEC: The First Ten Years, eds Jacoby G. H., Barnes J., p. 17
 Baldini L., Bucciantini N., Lalla N. D. *et al.* 2022, *SoftwareX*, 19, 101194
 Bentz M. C., Onken C. A., Street R., Valluri M. 2023, *Astrophys. J.*, 944, 29
 Boroson T. A., Green R. F. 1992, *Astrophys. J. Suppl.*, 80, 109
 Chartas G., Rhea C., Kochanek C. *et al.* 2016, *Astron. Nachr.*, 337, 356
 Condon J. J., Huang Z. P., Yin Q. F., Thuan T. X. 1991, *Astrophys. J.*, 378, 65
 Dewangan G. C., Tripathi P., Papadakis I. E., Singh K. P. 2021, *Mon. Not. R. Astron. Soc.*, 504, 4015

- Fabian A. C. 2012, *Ann. Rev. Astron. Astrophys.*, 50, 455
- Fabian A. C., Lohfink A., Belmont R., Malzac J., Coppi P. 2017, *Mon. Not. R. Astron. Soc.*, 467, 2566
- Fabian A. C., Zoghbi A., Ross R. R. *et al.* 2009, *Nature*, 459, 540
- Fedorova E., Hnatyk B., Del Popolo A., Vasylenko A., Voitsekhovskiy V. 2022, *Galaxies*, <https://doi.org/10.3390/galaxies10010006>
- Gianolli V. E., Kim D. E., Bianchi S. *et al.* 2023, arXiv e-prints, [arXiv:2303.12541](https://arxiv.org/abs/2303.12541)
- Haardt F., Maraschi L. 1991, *Astrophys. J. Lett.*, 380, L51
- Haardt F., Maraschi L. 1993, *Astrophys. J.*, 413, 507
- Haardt F., Maraschi L., Ghisellini G. 1994, *Astrophys. J. Lett.*, 432, L95
- Harrison F. A., Craig W. W., Christensen F. E. *et al.* 2013, *Astrophys. J.*, 770, 103
- Hartman R. C., Bertsch D. L., Bloom S. D. *et al.* 1999, *Astrophys. J. Suppl.*, 123, 79
- Ingram A., Ewing M., Marinucci A. *et al.* 2023, arXiv e-prints, [arXiv:2305.13028](https://arxiv.org/abs/2305.13028)
- Inoue Y., Doi A. 2018, *Astrophys. J.*, 869, 114
- Kamraj N., Brightman M., Harrison F. A. *et al.* 2022, *Astrophys. J.*, 927, 42
- Kang J.-L., Wang J.-X. 2022, *Astrophys. J.*, 929, 141
- Kang J.-L., Wang J.-X., Kang W.-Y. 2021, *Mon. Not. R. Astron. Soc.*, 502, 80
- Keek L., Ballantyne D. R. 2016, *Mon. Not. R. Astron. Soc.*, 456, 2722
- Kellermann K. I., Sramek R., Schmidt M., Shaffer D. B., Green R. 1989, *Astron. J.*, 98, 1195
- Lubiński P., Beckmann V., Gibaud L. *et al.* 2016, *Mon. Not. R. Astron. Soc.*, 458, 2454
- Lynden-Bell D. 1969, *Nature*, 223, 690
- Marinucci A., Muleri F., Dovciak M. *et al.* 2022, *Mon. Not. R. Astron. Soc.*, 516, 5907
- Matt G., Fabian A. C., Ross R. R. 1993, *Mon. Not. R. Astron. Soc.*, 264, 839
- Matt G., Perola G. C., Costa E., Piro L. 1989, in *ESA Special Publication, Vol. 296, Two Topics in X-Ray Astronomy, Vol. 1: X Ray Binaries. Vol. 2: AGN and the X Ray Background*, eds Hunt J., Battrick B., p. 991
- McKernan B., Yaqoob T. 2004, *Astrophys. J.*, 608, 157
- Middei R., Bianchi S., Marinucci A. *et al.* 2019, *Astron. Astrophys.*, 630, A131
- Murray N., Chiang J., Grossman S. A., Voit G. M. 1995, *Astrophys. J.*, 451, 498
- Padovani P. 2017, *Front. Astron. Space Sci.*, 4, 35
- Pal I., Stalin C. S. 2023, *Mon. Not. R. Astron. Soc.*, 518, 2529
- Pal I., Stalin C. S., Mallick L., Rani P. 2022, *Astron. Astrophys.*, 662, A78
- Pal I., Stalin C. S., Parker M. L., Agrawal V. K., Marchesi S. 2022, *Mon. Not. R. Astron. Soc.*, 517, 3341
- Petrucci P. O., Haardt F., Maraschi L. *et al.* 2001, *Astrophys. J.*, 556, 716
- Poutanen J., Svensson R. 1996, *Astrophys. J.*, 470, 249
- Poutanen J., Veledina A., Beloborodov A. M. 2023, *Astrophys. J. Lett.*, 949, L10
- Rani P., Stalin C. S. 2018, *Astrophys. J.*, 856, 120
- Rees M. J. 1984, *Ann. Rev. Astron. Astrophys.*, 22, 471
- Sanders D. B., Mirabel I. F. 1996, *Ann. Rev. Astron. Astrophys.*, 34, 749
- Shakura N. I., Sunyaev R. A. 1973, *Astron. Astrophys.*, 500, 33
- Steenbrugge K. C., Kaastra J. S., Sako M. *et al.* 2005, *Astron. Astrophys.*, 432, 453
- Tamborra F., Matt G., Bianchi S., Dovciak M. 2018, *Astron. Astrophys.*, 619, A105
- Tortosa A., Bianchi S., Marinucci A., Matt G., Petrucci P. O. 2018, *Astron. Astrophys.*, 614, A37
- Urry C. M., Padovani P. 1995, *Publ. Astron. Soc. Pac.*, 107, 803
- Ursini F., Matt G., Bianchi S. *et al.* 2021, *Mon. Not. R. Astron. Soc.*, 510, 3674
- Ursini F., Boissay R., Petrucci P. O. *et al.* 2015, *Astron. Astrophys.*, 577, A38
- Ursini F., Petrucci P. O., Matt G. *et al.* 2016, *Mon. Not. R. Astron. Soc.*, 463, 382
- Ursini F., Marinucci A., Matt G. *et al.* 2023, *Mon. Not. R. Astron. Soc.*, 519, 50
- Véron-Cetty M. P., Véron P. 2010, *Astron. Astrophys.*, 518, A10
- Weisskopf M. C., Soffitta P., Baldini L. *et al.* 2022, *J. Astron. Telesc. Instrum. Syst.*, 8, 026002
- Willingale R., Starling R. L. C., Beardmore A. P., Tanvir N. R., O'Brien P. T. 2013, *Mon. Not. R. Astron. Soc.*, 431, 394
- Willmer C. N. A., Focardi P., Chan R., Pellegrini P. S., da Costa N. L. 1991, *Astron. J.*, 101, 57
- Zhang W., Dovčaniak M., Bursa M. 2019, *Astrophys. J.*, 875, 148
- Zoghbi A., Matt G., Miller J. M. *et al.* 2017, *Astrophys. J.*, 836, 2